

# nature



## WAKING UP TO GLOBAL WARMING

The rodent linking climate  
change to population trends

ECOSYSTEM BALANCE

Who needs mosquitoes?

GRAPHENE

Making nanoribbons with  
atomic precision

DIABETES AND OBESITY

Two drugs in one?

## LETTERS

# Coupled dynamics of body mass and population growth in response to environmental change

Arpat Ozgul<sup>1</sup>, Dylan Z. Childs<sup>2</sup>, Madan K. Oli<sup>3</sup>, Kenneth B. Armitage<sup>4</sup>, Daniel T. Blumstein<sup>5</sup>, Lucretia E. Olson<sup>5</sup>, Shripad Tuljapurkar<sup>6</sup> & Tim Coulson<sup>1</sup>

Environmental change has altered the phenology, morphological traits and population dynamics of many species<sup>1,2</sup>. However, the links underlying these joint responses remain largely unknown owing to a paucity of long-term data and the lack of an appropriate analytical framework<sup>3</sup>. Here we investigate the link between phenotypic and demographic responses to environmental change using a new methodology and a long-term (1976–2008) data set from a hibernating mammal (the yellow-bellied marmot) inhabiting a dynamic subalpine habitat. We demonstrate how earlier emergence from hibernation and earlier weaning of young has led to a longer growing season and larger body masses before hibernation. The resulting shift in both the phenotype and the relationship between phenotype and fitness components led to a decline in adult mortality, which in turn triggered an abrupt increase in population size in recent years. Direct and trait-mediated effects of environmental change made comparable contributions to the observed marked increase in population growth. Our results help explain how a shift in phenology can cause simultaneous phenotypic and demographic changes, and highlight the need for a theory integrating ecological and evolutionary dynamics in stochastic environments<sup>4,5</sup>.

Rapid environmental change, largely attributed to anthropogenic influences, is occurring at an unprecedented rate<sup>6,7</sup>. Concurrent with environmental change, there have been changes in the phenology<sup>8</sup>, geographic distribution<sup>9</sup>, phenotypic trait distributions and population dynamics<sup>10</sup> of wildlife species, particularly those living in extreme environments including high altitude or latitude ecosystems<sup>2,11</sup>. However, the proximate causes that generate such change are rarely identified, and most analyses are phenomenological<sup>2</sup>. Population-level responses to environmental change can be of several types: genetic changes occur as a result of directional selection on heritable traits or drift<sup>12,13</sup>; life-history and quantitative traits can shift as a result of both a plastic response to environmental change<sup>14,15</sup> and changing selection pressures<sup>16–18</sup>; and population size can change with changing demographic rates<sup>19,20</sup>. Each of these processes depends on the association between phenotypic traits and survival, reproduction, trait development among survivors and the distribution of traits among newborns<sup>21</sup>. Understanding the effects of environmental change on populations consequently requires insight into how phenotype–demography relationships are altered and how these changes affect the distribution of phenotypic traits, life history and population growth<sup>22,23</sup>.

In this study, we use a long-term data set from a hibernating sciurid rodent inhabiting a subalpine habitat to investigate how environmental change has affected phenotypic traits and population dynamics (Supplementary Fig. 1). We used 33 years (1976–2008) of

individual-based life-history and body-mass data collected from a yellow-bellied marmot (*Marmota flaviventris*) population located in the Upper East River Valley, Colorado, USA. We used data only from the female segment of the population because maternity, unlike paternity, is known with confidence for each pup and most males disperse by the end of their second year. We focus on body mass as the focal phenotypic trait because marmot life history, particularly survival during hibernation and reproduction on emergence, is heavily dependent on this trait<sup>24,25</sup>.

Environmental change has influenced several aspects of marmot phenology<sup>8</sup>. Marmots have been emerging earlier from hibernation<sup>8</sup> and giving birth earlier in the season (Fig. 1a), which allows individuals more time to grow until immergence into hibernation. Using body-mass measurements from repeated captures during each summer and mixed-effects models, we estimated body mass on 1 August for each individual in the population in each year (Supplementary Fig. 2). Despite annual fluctuations, there has been a shift in the mean body mass in older age classes; for example, the mean body mass for 2-year-old and older adults increased from 3,094.4 g (standard error of the mean (s.e.m.) = 28.9) during the first half of the study to 3,433.0 g (s.e.m. = 28.0) during the second half (Fig. 1b). Meanwhile, population size fluctuated around a stable equilibrium until 2001, followed by a steady increase over the last seven years (Fig. 1c). A nonlinear (weighted) least-squares analysis indicated a break-point in population dynamics at year 2000.9 (s.e.m. = 1.12,  $P < 0.001$ ). The regression slopes from this analysis reveal that the population size increased on average by 0.56 (s.e.m. = 0.45,  $P = 0.22$ ) marmots per year between 1976 and 2001 and by 14.2 marmots per year subsequently (s.e.m. = 3.17,  $P < 0.01$ ), indicating a major shift in the population dynamics. To examine these demographic and phenotypic changes, we compared body-mass–demography associations between pre-2000 and post-2000 years. We included a one-year lag because body condition is expected to influence population size (through survival and reproduction) one year later. It is notable that the change in population growth rate occurred more suddenly than the change in mean body mass (Fig. 1b, c). Nonetheless, the majority of the highest mean body masses were observed during the last decade, particularly for adults, indicating that gradual changes in the environment may have passed a threshold leading to a gradual shift in the body mass and an abrupt shift in the demographic regime. Interestingly, other aspects of marmot habitat, including flowering rates of tall bluebells (*Mertensia ciliata*), also changed around 2000 (Supplementary Fig. 3).

Our next objective was to understand why these joint changes were observed. We used mark–recapture methods<sup>26</sup> and generalized linear and additive models<sup>27</sup> to identify the most parsimonious functions

<sup>1</sup>Department of Life Sciences, Imperial College London, Ascot, Berkshire SL5 7PY, UK. <sup>2</sup>Department of Animal and Plant Sciences, University of Sheffield, Sheffield S10 2TN, UK. <sup>3</sup>Department of Wildlife Ecology and Conservation, University of Florida, Gainesville, Florida 32611, USA. <sup>4</sup>Department of Ecology and Evolutionary Biology, University of Kansas, Lawrence, Kansas 66045, USA. <sup>5</sup>Department of Ecology and Evolutionary Biology, University of California, Los Angeles, California 90095, USA. <sup>6</sup>Department of Biology, Stanford University, Stanford, California 94305, USA.

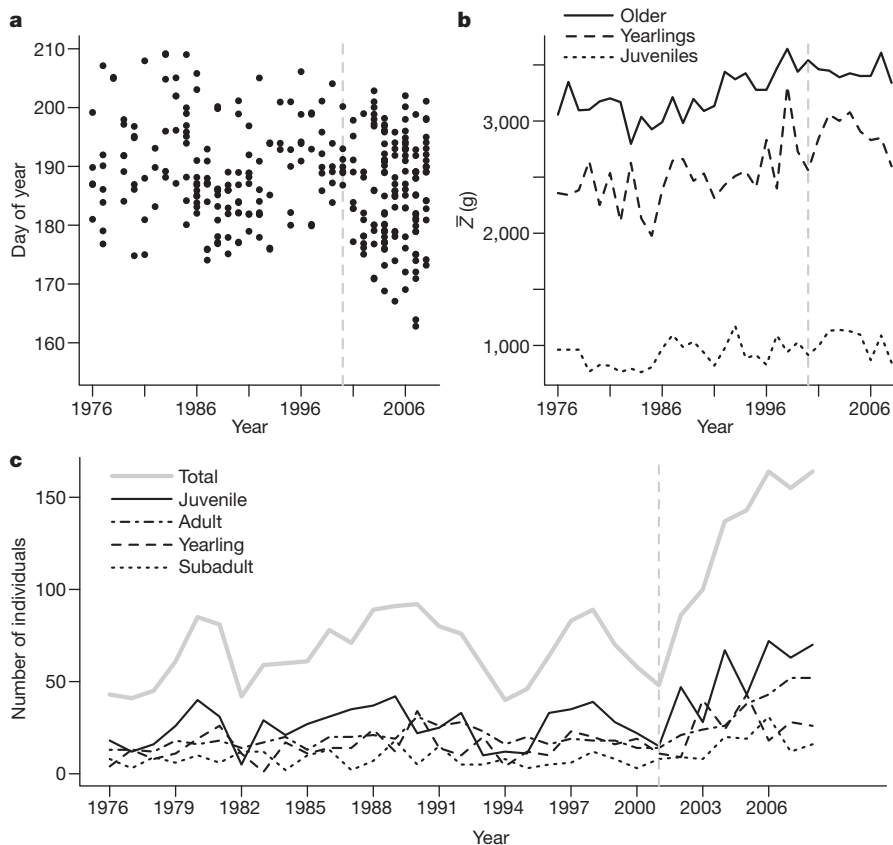


**Figure 1 | Trends in the phenology, mean phenotypic trait and demography for females of the yellow-bellied marmot population. a–c,** Time of weaning ( $-0.17$  days per year,  $P < 0.01$ ) (a), mean 1 August mass ( $\bar{Z}$ ) (b), and abundance in each age class (c). The four age classes are juvenile ( $<1$  yr),

yearling (1 yr-old), subadult (2 yrs-old) and adult ( $\geq 3$  yrs-old). Subadult and adult masses are combined (older) in b. Vertical dotted lines delineate different phases of population dynamics.

describing associations between body-mass and demographic (survival, reproduction probability and litter size) and trait-transition (growth and offspring body mass) rates. We also tested for the effects of age class and study period on these rates. Body mass had a significant positive influence on most rates in both periods (Supplementary Figs 4–7). Moreover, the form of some of the body-mass–rate functions also changed over time. Heavier marmots, particularly adults, survived better in later years (Fig. 2a). Both mean juvenile growth (from the first to second August of life) and the dependence of growth on mass increased in later years (Fig. 2b); the resulting increase in growth was much greater among smaller juveniles. In addition, heavier females had a higher chance of reproducing in later years (Fig. 2c).

To understand the population dynamic and phenotypic consequences of these changes, we used a recently developed method, an integral projection model (IPM)<sup>28,29</sup>, which projects the distribution of a continuous trait based on demographic and trait transition functions. Using the fitted functions relating body mass to each rate, we parameterized two IPMs, one for the pre-2000 period and one for after 2000. Eigenanalysis of the two IPMs captured the observed change in the dynamics: the annual asymptotic population growth rate ( $\lambda$ ) increased from an approximately stable ( $\lambda = 1.02$ ) in the earlier period to a rapidly increasing ( $\lambda = 1.18$ ) in the later period (Fig. 1c). The stable mass distributions for each of the periods captured the observed increase in body mass in both juveniles (38.2 g, 4.2%) and older age classes (166.7 g, 5.8%) (Fig. 3a). To identify which demographic or trait transition function had contributed most to the observed increase in population growth rate, we performed a retrospective perturbation analysis of the two IPMs. The observed increase in population growth rate was predominantly due to changes in the adult survival and juvenile growth functions (Fig. 3b).

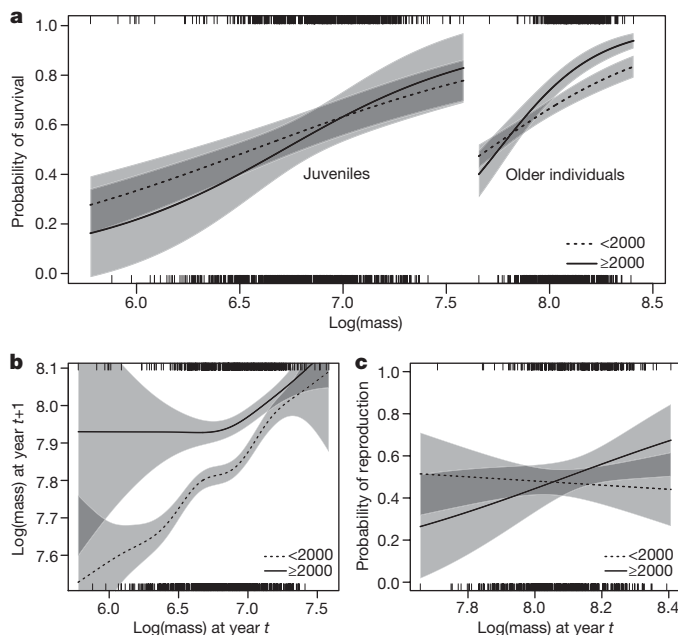


**Figure 2 | The relationship between body mass and demographic and trait transition rates. a–c,** Effect of body mass on survival (a), juvenile growth (b) and adult reproduction (c) for pre-2000 ( $<2000$ ) and post-2000 ( $\geq 2000$ ) years. Shaded areas indicate the 95% confidence intervals, and rugs below and above the graph represent the distribution of the body mass data for  $<2000$  and  $\geq 2000$ , respectively.

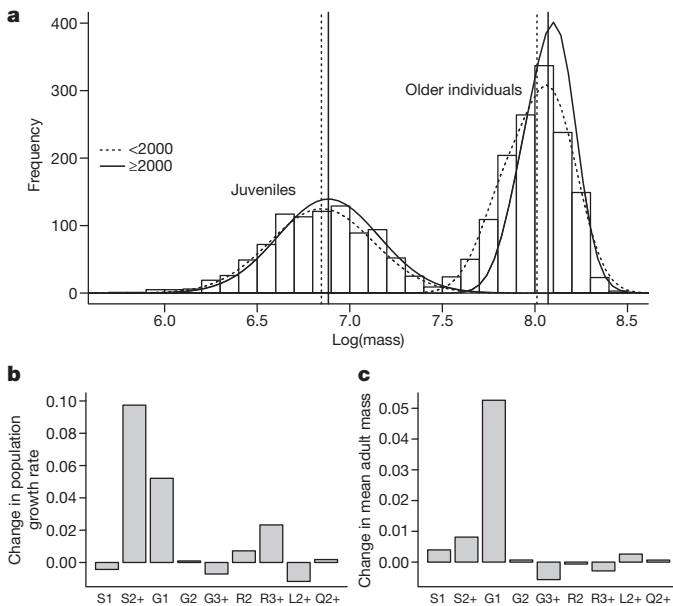


**Figure 3 | Trait-based analysis of the population dynamics.** **a**, Stable August log-body-mass distributions (lines) for juveniles and older individuals for  $<2000$  and  $\geq 2000$ . Vertical lines show the mean body masses. Bars indicate the actual observed distribution over the entire study period. **b**, **c**, Retrospective perturbation analysis of the integral projection model gives the relative contribution of each function to population growth (**b**) and to change in mean adult body mass (**c**) from the  $<2000$  to the  $\geq 2000$  period (G, growth; L, litter size; Q, offspring mass; R, reproduction probability; S, survival; numbers indicate the age classes).

The increase in mean adult survival was the key demographic factor underlying the observed shift in population dynamics between the two periods. It could have been caused by two non-mutually exclusive processes: a change in the relationship between August mass and survival, and a change in mean August mass in each age class. To understand the relative contributions of these two processes, we estimated three mean survival rates for each age class using: (1) the earlier period's survival curve and trait distribution,  $S_1(Z_1)$ ; (2) the earlier period's survival curve and the later period's trait distribution,  $S_1(Z_2)$ ; and (3), the later period's survival curve and trait distribution,  $S_2(Z_2)$ . The difference between (2) and (1) versus the difference between (3) and (2) indicates the contributions of the change in mean mass versus the change in survival curve. The juvenile survival did not change substantially, yet the observed small increase was caused by a change in the mass distribution. For older marmots, both processes made comparable contributions to the increase in survival (Fig. 4). The change in the mass distribution contributed slightly more to the increase in yearling survival, whereas the change in the survival curve contributed more to the increase in subadult and adult survival. As the increase in the survival of older individuals is the prominent cause of the observed population increase, both the faster growth of marmots and the change in the relationship between August mass and survival must have had an important role in the observed shift in population dynamics.

Finally, to understand the processes underlying the observed phenotypic change, we decomposed the change in mean body mass,  $\Delta \bar{Z}$ , into contributions from selection and other processes using the recently developed age-structured Price equation<sup>21</sup> (Supplementary Fig. 8A). The mean annual growth of juveniles increased from  $1,523.7 \text{ g year}^{-1}$  (s.e.m. = 45.1) for years before 2000 to  $1,847.4 \text{ g year}^{-1}$  (s.e.m. = 78.1) for those after 2000 ( $P < 0.01$ ). This faster growth from the first to the second August of life resulted in higher mean body masses in the older age classes, as also demonstrated by the retrospective perturbation analysis of the IPMs (Fig. 3c). The temporal change in mean body mass for the whole

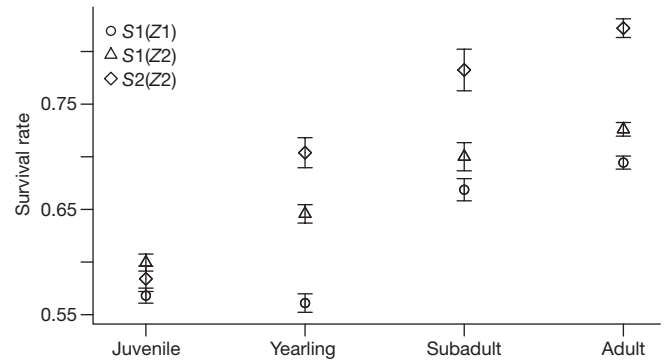


**Figure 4 | Contributions of the changes in mean mass ( $Z_1$  to  $Z_2$ ) and mass-survival relationship ( $S_1$  to  $S_2$ ) to the increase in mean survival from  $<2000$  to  $\geq 2000$ .** The proximity of the triangle ( $S_1(Z_2)$ ) to the circle ( $S_1(Z_1)$ ) versus to the diamond ( $S_2(Z_2)$ ) indicates the contributions of the change in mean mass versus the change in survival curve for each age class. Confidence intervals indicate the process variation estimated using the particular mass distribution and survival function.

population over the 33 years was predominantly explained by changes in the mean growth rate contributions (52%), with selection-related terms contributing only 3% (Supplementary Fig. 8B), indicating that the change in body mass is not the result of a change in selection operating on the trait.

How can we interpret these results? The population-level response to environmental change was mediated to a large extent through environmental influences on body mass. The increase in the length of the growing season has altered the phenology; marmots are now born earlier and they have more time to grow until the next hibernation. This increase in juvenile growth has caused an increase in body mass in all age classes. Yet, most of this change was an ecological (plastic) rather than an evolutionary response to environmental change as also seen in Soay sheep on St Kilda<sup>22</sup>. This increase in body mass and the length of the growing season has also altered the functional dependence of vital rates on body mass. Heavier marmots now survive and reproduce better than they once did, and this has led to a rapid increase in population size in recent years.

A simultaneous response to environmental change in phenology, phenotypic traits and population dynamics seems to be commonplace in nature<sup>2</sup>. We have demonstrated how such joint dynamics can be investigated, and have shown how changes in phenotypic traits and population dynamics can be intimately linked. If we are to understand the biological consequences of environmental change it will prove necessary to gain further insight into these linkages. Despite this, we do not completely understand why the body-mass–demography associations changed as markedly as we observe. This means that predicting future change will prove more challenging than characterizing past change. We suspect that the observed increase in marmot survival is likely to be a short-term response to the lengthening growing season. Longer-term consequences may depend on whether long, dry summers become more frequent, as this would decrease growth rates and increase mortality rates. Characterizing observed interactions between environment, phenotypic traits and demography is challenging; accurately predicting how they may change in the future will almost certainly require a mechanistic understanding of how environmental change impacts resource availability as well as individual energy budgets<sup>30</sup>.

## METHODS SUMMARY

This study was conducted in the Upper East River Valley near the Rocky Mountain Biological Laboratory, Gothic, Colorado ( $38^\circ 57' \text{ N}$ ,  $106^\circ 59' \text{ W}$ , approximately 2,950 m elevation). We used data from 1,190 live-trapped females from 1976 to 2008. The body-mass data were collected from each individual at several captures during May–September. We used a generalized mixed model for each age class to estimate the 1 August (214th day-of-year) body masses accounting for the random

effects of year, site and individual identity. For the analysis of stage-specific survival functions, we used a multistate mark–recapture model where we tested for the individual and interaction effects of body mass (as a time-varying individual covariate) and the study period. We used generalized linear and additive models for the rest of the demographic and transition functions and tested for linear, nonlinear and interaction effects of body mass, age class and study period. Using the most parsimonious functions relating body mass to each demographic and trait-transition rate, we parameterized two  $400 \times 400$  stage- and mass-structured integral projection matrices (one for the pre-2000 period and one for after 2000), each consisting of 4 stages and 100 mass intervals. For the retrospective perturbation analysis, we created 512 IPMs representing all possible combinations of change among the nine functions and estimated the corresponding change in  $\lambda$ . The same method was used to estimate the contribution of each functional change to the change in mean adult mass. Using the age-structured Price equation, we decomposed the observed change in mean body mass into exact contributions from selection and other processes.

**Full Methods** and any associated references are available in the online version of the paper at [www.nature.com/nature](http://www.nature.com/nature).

**Received 11 February; accepted 28 May 2010.**

- Walther, G. *et al.* Ecological responses to recent climate change. *Nature* **416**, 389–395 (2002).
- Parnesan, C. Ecological and evolutionary responses to recent climate change. *Annu. Rev. Ecol. Syst.* **37**, 637–669 (2006).
- Stenseth, N. & Mysterud, A. Climate, changing phenology, and other life history traits: Nonlinearity and match/mismatch to the environment. *Proc. Natl Acad. Sci. USA* **99**, 13379–13381 (2002).
- Coulson, T., Benton, T. G., Lundberg, P., Dall, S. R. X. & Kendall, B. E. Putting evolutionary biology back in the ecological theatre: a demographic framework mapping genes to communities. *Evol. Ecol. Res.* **8**, 1155–1171 (2006).
- Chevin, L. M., Lande, R. & Mace, G. M. Adaptation, plasticity and extinction in a changing environment: Towards a predictive theory. *PLoS Biol.* **8**, e1000357 (2010).
- Intergovernmental Panel on Climate Change. *The Physical Science Basis: Contribution of Working Group I to the Fourth Assessment Report of the IPCC.* (Cambridge Univ. Press, 2007).
- Karl, T. & Trenberth, K. Modern global climate change. *Science* **302**, 1719–1723 (2003).
- Inouye, D. W., Barr, B., Armitage, K. B. & Inouye, B. D. Climate change is affecting altitudinal migrants and hibernating species. *Proc. Natl Acad. Sci. USA* **97**, 1630–1633 (2000).
- Thomas, C. & Lennon, J. Birds extend their ranges northwards. *Nature* **399**, 213 (1999).
- Pounds, J. A. *et al.* Widespread amphibian extinctions from epidemic disease driven by global warming. *Nature* **439**, 161–167 (2006).
- Jenouvrier, S. *et al.* Demographic models and IPCC climate projections predict the decline of an emperor penguin population. *Proc. Natl Acad. Sci. USA* **106**, 1844–1847 (2009).
- Fisher, R. A. *The Genetical Theory of Natural Selection* (Oxford Univ. Press, 1958).
- Bradshaw, W. & Holzapfel, C. Evolutionary response to rapid climate change. *Science* **312**, 1477–1478 (2006).
- Via, S. *et al.* Adaptive phenotypic plasticity: consensus and controversy. *Trends Ecol. Evol.* **10**, 212–217 (1995).
- Reale, D., McAdam, A. G., Boutin, S. & Berteaux, D. Genetic and plastic responses of a northern mammal to climate change. *Proc. R. Soc. Lond. B* **270**, 591–596 (2003).
- Lande, R. Natural selection and random genetic drift in phenotypic evolution. *Evolution* **30**, 314–334 (1976).
- Berthold, P., Helbig, A. J., Mohr, G. & Querner, U. Rapid microevolution of migratory behavior in a wild bird species. *Nature* **360**, 668–670 (1992).
- Gienapp, P., Teplitsky, C., Alho, J. S., Mills, J. A. & Merila, J. Climate change and evolution: disentangling environmental and genetic responses. *Mol. Ecol.* **17**, 167–178 (2008).
- Tuljapurkar, S. & Caswell, H. *Structured-Population Models in Marine, Terrestrial, and Freshwater Systems* (Chapman & Hall, 1997).
- Sæther, B.-E. *et al.* Population dynamical consequences of climate change for a small temperate songbird. *Science* **287**, 854–856 (2000).
- Coulson, T. & Tuljapurkar, S. The dynamics of a quantitative trait in an age-structured population living in a variable environment. *Am. Nat.* **172**, 599–612 (2008).
- Ozgul, A. *et al.* The dynamics of phenotypic change and the shrinking sheep of St. Kilda. *Science* **325**, 464–467 (2009).
- Pelletier, F., Clutton-Brock, T., Pemberton, J., Tuljapurkar, S. & Coulson, T. The evolutionary demography of ecological change: linking trait variation and population growth. *Science* **315**, 1571–1574 (2007).
- Armitage, K. B., Downhower, J. F. & Svendsen, G. E. Seasonal changes in weights of marmots. *Am. Midl. Nat.* **96**, 36–51 (1976).
- Armitage, K. B. in *Wild Mammals of North America: Biology, Management, and Conservation* 2nd edn (eds Feldhamer, G. A., Thompson, B. C. & Chapman, J. A.) 188–210 (Johns Hopkins Univ. Press, 2003).
- Brownie, C., Hines, J. E., Nichols, J. D., Pollock, K. H. & Hestbeck, J. B. Capture–recapture studies for multiple strata including non-Markovian transitions. *Biometrics* **49**, 1173–1187 (1993).
- Wood, S. N. *Generalized Additive Models: An Introduction with R.* (Chapman & Hall, 2006).
- Easterling, M. R., Ellner, S. P. & Dixon, P. M. Size-specific sensitivity: Applying a new structured population model. *Ecology* **81**, 694–708 (2000).
- Ellner, S. P. & Rees, M. Integral projection models for species with complex demography. *Am. Nat.* **167**, 410–428 (2006).
- Humphries, M., Umbanhowar, J. & McCann, K. Bioenergetic prediction of climate change impacts on northern mammals. *Integr. Comp. Biol.* **44**, 152 (2004).

**Supplementary Information** is linked to the online version of the paper at [www.nature.com/nature](http://www.nature.com/nature).

**Acknowledgements** We thank the ‘marmoteers’ who participated in collecting the long-term data, Rocky Mountain Biological Laboratory for providing the field facilities, B. Barr and D. Inouye for providing additional information on climate and plant phenology, and L. M. Chevin, J. A. Hostetler, D. Inouye, N. J. Singh and I. M. Smallegange for comments. This work was funded by NERC, the Wellcome Trust, NSF, NIH and NIA.

**Author Contributions** K.B.A. and D.T.B. led the long-term study; K.B.A., D.T.B., L.E.O. and A.O. collected data; A.O. and T.C. conceived the ideas for the paper and its structure; A.O., D.Z.C., T.C., M.K.O. and S.T. designed the analyses; A.O. and D.Z.C. conducted the analyses; A.O. wrote the manuscript; all authors discussed the results and commented on the manuscript.

**Author Information** Reprints and permissions information is available at [www.nature.com/reprints](http://www.nature.com/reprints). The authors declare no competing financial interests. Readers are welcome to comment on the online version of this article at [www.nature.com/nature](http://www.nature.com/nature). Correspondence and requests for materials should be addressed to A.O. (a.ozgul@imperial.ac.uk).

## METHODS

**The study system.** The yellow-bellied marmot is a large, diurnal, burrow-dwelling rodent, occupying montane regions of western North America<sup>25,31</sup>. The species hibernates from September or October to April or May, during which time individuals lose approximately 40% of their body mass<sup>25</sup>. The need to mobilize energy for reproduction and then prepare for hibernation in a short time period accounts for the energy conservative physiology of this species<sup>32,33</sup>. The critical factor determining winter survival and subsequent reproductive success is the amount of fat accumulated before hibernation<sup>34,35</sup>. On emergence all age classes start gaining mass at the rate of about 12–14 g day<sup>-1</sup>. The annual cycle is a major constraint on population dynamics. The need to satisfy the energy requirements for hibernation limits reproduction to a single annual event occurring immediately after emergence. The short active season combined with large body size delays reproductive maturity until two years of age<sup>36</sup>.

This study was conducted in the Upper East River Valley near the Rocky Mountain Biological Laboratory, Gothic, Colorado (38° 57' N, 106° 59' W). Data were collected from 17 distinct sites within the study area<sup>37,38</sup>. From 1962 to 2008, yellow-bellied marmots were live-trapped at each site throughout the active season (May–September) and individually marked using numbered ear tags<sup>39</sup>. Animal identification number, sex, mass and reproductive condition were recorded at each capture. Ages for females that were captured as juveniles were known, whereas ages for other females were estimated based on body mass ( $\leq 2$  kg = yearling,  $> 2$  kg = adult)<sup>24</sup>. In this study, we omitted the years before 1976 owing to lower sampling effort.

Survival and reproduction are affected by the length of the active season, which varies from year to year as a consequence of variation in the onset and/or termination of snow cover<sup>40,41</sup>. The length of the growing season also varies among marmot sites over a distance of 4.8 km in the Upper East River Valley where the greatest difference in elevation between colonies is 165 m. The biology of yellow-bellied marmots in Colorado is described in further detail elsewhere<sup>25,39</sup>.

**Estimation of 1 August body mass.** Marmot life history is tightly related to the circannual rhythm<sup>25</sup>. As marmots lose approximately 40% of their body mass during hibernation<sup>25</sup> and females give birth in late May, the mean body mass changes substantially over the active season and among age classes. Furthermore, the study area includes several sites with different elevations and aspects and the environmental conditions vary among years, causing variation in mean body mass among sites and years at a given date. In this study, we focus on the estimated 1 August body mass as it provides the best trade-off between data availability and biological significance. The trapping data until mid-August is sufficient to provide a good estimate of body mass, from which point on the data become sparse in most years (Supplementary Fig. 2). August mass is biologically significant for several reasons: (1) it is beyond the influence of the previous hibernation, particularly for non-reproductive stages; (2) marmots are weaned no later than mid-July and there is no reproductive activity until the following spring so 1 August mass is not confounded by pregnancy; (3) as the plant mass growth peaks in mid-July<sup>33,42</sup>, growth plateaus in early August for non-reproductive adults, mid-August for juveniles and late August for reproductive females<sup>25,43,44</sup>. Therefore, it covers most of the critical period for individual growth.

The body-mass data were collected from each individual at several captures throughout the active season. Individuals were captured an average of 3.12 times in a given year with a maximum of 7.45 captures in 2003. We grouped individuals into four age classes (*a*): juvenile (*a* = 1, year 0–1), yearling (*a* = 2, year 1–2), subadult (*a* = 3, year 2–3), and adult (*a* = 4, year  $> 3$ ). To estimate the 1 August body mass for each individual per year, we constructed a general linear mixed model including the fixed effect of day of year on body mass, and the random effects of year, site and individual identity. Models were fitted with the lme4 package<sup>45</sup>. A separate model was fitted to each age class and random deviations were incorporated in both the intercept and the (linear) day-of-year term for all three random effects. Because it includes several ages ( $\geq 3$  yrs old), the adult model also incorporates a random 'observation age' term (nested within individual) to accommodate individual level variation in size among successive observation years. We did not attempt to determine whether specific variance components were significantly different from zero. This is unnecessary when the goal of modelling is prediction; negligible sources of variation are simply estimated to be near zero and thus to contribute little to predicted values. For all four age classes we compared a set of nested models for the fixed effects structure, which incorporated up to third-order polynomial terms for day of year. The set of models constructed for adults also considered models with a fixed effect of age and the interaction of age with day of year. Fixed effect structures were compared using likelihood ratio tests<sup>46</sup>. Some caution is required when applying likelihood ratio tests to examine the significance of fixed effects as these

are known to be anticonservative. Fortunately, all of the results we report were highly significant.

The most parsimonious models included second-order polynomial terms for day of year in juveniles and yearlings, and only the linear effect in subadults and adults (Supplementary Fig. 2). The most parsimonious adult model also included an age effect but not the interaction term with day of year. For example, in juveniles and yearlings the expected mass of an individual at observation *i* is given by:

$$E[\mu_i] = (\beta_0 + u_{fm(i),0} + v_{yr(i),0} + w_{st(i),0}) + (\beta_1 + u_{fm(i),1} + v_{yr(i),1} + w_{st(i),1})D + \beta_2 D^2$$

where *D* is the day of year; *u*, *v* and *w* refer to the random female, year and site effects, respectively;  $\beta_1$  and  $\beta_2$  are the linear and quadratic fixed effect terms for day of year, respectively; and  $\beta_0$  is the global intercept. In the random terms, the first subscript (for example, *yr*(*i*)) can be viewed as a mapping function referencing the appropriate random effect level for observation *i*, and the second subscript references the random intercept or slope term as appropriate. Using the fitted models, we predicted the 1 August (214th day-of-year) mass for each individual conditional on the predicted random effects given by the best linear unbiased predictors (BLUPs). We used these estimated 1 August masses for the rest of the analyses.

### Relationship between body mass and demographic and trait transition rates.

To understand the link between phenotypic dynamics and population dynamics, we examined the relationship between body mass and each of the five demographic and trait transition rates using the long-term individual-based data. The demographic rates are, (1) the survival from one year to the next (0 or 1), (2) reproducing the following year conditional on survival (0 or 1), and (3) litter size conditional on reproduction ( $\geq 1$ ); whereas the trait-transition rates are, (4) the ontogenic growth from one August to the next, and (5) the average 1 August body mass of the offspring (that is, juvenile) produced to the next year. It is important to note that most of the juvenile growth (from its first to second August of life) occurs after individuals emerge from their first hibernation as yearlings; similarly, most of the yearling growth (from its second to third August of life) occurs after individuals emerge from their second hibernation as subadults.

For the analysis of survival rates, we used a multistate mark-recapture model<sup>26</sup> implemented using Program MARK<sup>47</sup> with the RMark interface<sup>48</sup>, where we tested for the effect of body mass (as a time-varying individual covariate) on stage-specific survival rates. For the rest of the rates, the functions were characterized using generalized linear and additive models (GAMs)<sup>27</sup>, as the associations between quantitative traits and demographic rates could be nonlinear<sup>49,50</sup>. For each rate, the number of demographic classes was determined by comparing models with different stage structures using Akaike's information criterion<sup>51</sup>.

We next tested for linear, nonlinear, and two-way interaction effects of the current August body mass, age class and study period. All rates, except for litter size and offspring mass, showed significant changes from the earlier to the later period (Supplementary Table 1), and body mass had a significant influence on all rates during both periods. Moreover, the relationship between body mass and some of the demographic and trait-transition rates significantly differed between the two periods (Supplementary Figs 4–7). The general models describing the demographic and trait-transition rates are summarized in Supplementary Table 1.

**Construction of the integral projection models.** The analysis of demographic and trait-transition rates described earlier showed that individual fates are influenced by their body mass and age class. To accommodate both factors in an efficient manner we constructed a stage- and mass-structured IPM. General IPMs project the distribution of discrete and continuous trait-structured population in discrete time. Their main advantage is that they allow parsimonious modelling of changes in both the phenotypic distribution and population growth rate based on easily estimated demographic and trait-transition functions<sup>28</sup>. Theory for general IPMs in a constant environment and an example application of an age- and size-structured model can be found in refs 29 and 52, respectively. Using the most parsimonious functions relating body mass to each demographic and trait-transition rate, we parameterized two IPMs, one for earlier ( $< 2000$ ) and one for later ( $\geq 2000$ ) years.

The two main elements of an IPM are the projected trait distributions for each stage class and the projection kernel components. Our IPM tracks the distribution of body mass in juvenile (*a* = 1), yearling (*a* = 2), subadult (*a* = 3) and adult (*a* = 4) stages. For a general stage class *a*, the number of individuals in the mass range  $[x, x + dx]$  at time *t* is denoted by  $n_a(x, t)$ . The dynamics of  $n_a(x, t)$  are governed by a set of coupled integral equations:

$$n_1(y, t + 1) = \sum_{a=2}^4 \int_{\Omega} F_a(y, x) n_a(x, t) dx$$

$$n_{a+1}(y, t + 1) = \int_{\Omega} P_a(y, x) n_a(x, t) dx \quad (\text{for } a = 1, 2, 3)$$

$$n_4(y, t + 1) = \int_{\Omega} P_3(y, x) n_3(x, t) dx + \int_{\Omega} P_4(y, x) n_4(x, t) dx$$

where  $\Omega$  is a closed interval characterizing the mass domain,  $F_a(y, x)$  are recruitment kernels that determine the contribution of juvenile, subadult and adult stages to the next generation, and  $P_a(y, x)$  are survival-growth kernels that determine the transitions among (or in the case of adults, within) the four life stages.

These kernels are implied directly by the statistical analysis of the data; the necessary functions are already parameterized for the two periods and summarized in Supplementary Table 1. The survival-growth kernel for individuals of age  $a$  is given by:

$$P_a(y, x) = S_a(x) G'_a(y, x)$$

An individual that remains in the population must survive over winter and grow. The prime notation in the growth kernel is present to highlight that this function is not the same object as the corresponding demographic growth model in Supplementary Table 1, but rather it is the conditional distribution of  $y$  given  $x$  (which is easily derived from the demographic growth model). The recruitment kernels are given by:

$$F_a(y, x) = S_a(x) R_a(x) L_a(x) Q'_a(y, x)$$

Reading from left to right, we see that to contribute a juvenile to the population in the following summer, a current individual with mass  $x$  must survive over winter and successfully reproduce in the following summer, giving rise to female recruits with mass  $y$ , the number and size of which depends on the reproducing adults' size. The prime notation present in the identifier of the offspring mass kernel serves the same purpose as that in the adult growth kernel above. The model only accounts for females, thus  $L_a(x)$  is the number of female offspring. Having specified the survival-growth and fecundity kernels, the model is now complete.

Sequential iteration of the IPM entails repeated numerical integration. To achieve this, we used a simple method called the midpoint rule. This method constructs a discrete approximation of the IPM on a set of 'mesh points' and then uses matrix multiplication to iterate the model. Similarly, computation of the asymptotic growth rate and stable age  $\times$  mass distribution is achieved by following the common procedures for a matrix projection model<sup>53</sup>. A detailed explanation of the midpoint rule has been previously given<sup>29</sup>. The accuracy of the method depends on the size of the mesh; increasing this improves the numerical accuracy of the approximation. We chose to divide the body mass interval into 50 mass classes, as this ensures that the population growth rate calculations are accurate to at least three decimal places.

**Retrospective perturbation analysis of the IPM.** To identify which one of the nine demographic and trait transition functions (Supplementary Table 1) contributed the most to the observed increase in  $\lambda$  from the earlier to the later period, we performed a retrospective perturbation analysis of the two IPMs. We first created a design matrix with nine columns representing all the functions (Supplementary Table 1) and 512 rows representing all possible combinations of change among these nine functions. The entries of the design matrix are 0 or 1, indicating whether the function was parameterized using  $<2000$  or  $\geq 2000$  data, respectively. Next, for each combination, we created an IPM and estimated the corresponding  $\lambda$ . Using the dummy coding for each of the nine functions as binary explanatory variables and  $\lambda$  as the response variable, we tested for the main effects of and two-way interactions between each of the nine functions. The main-effects model explained a substantial amount of the variation in  $\lambda$  ( $R^2 = 98.7\%$ ); therefore, we ignored the two-way interactions. The resulting regression effect sizes denote the change in  $\lambda$  contributed by the change in each of the nine demographic and trait transition components. Similarly, we estimated the contribution of each functional change to the mean adult mass by estimating a mean adult mass from the stable size distribution (right eigenvector) for each combination and applying the same methodology outlined above.

**The age-structured Price equation.** To understand the processes underlying the observed phenotypic change, we decomposed the change in mean body mass,

$\Delta \bar{Z}$ , into contributions from selection and other processes using the age-structured Price equation<sup>21,22</sup>. The exact change in mean value of a trait over a time step,  $\Delta \bar{Z}(t) = \bar{Z}(t+1) - \bar{Z}(t)$ , is decomposed into seven contributions. The mathematical details have been previously provided<sup>21,22</sup>. Here we provide further details on the interpretation of terms in Supplementary Fig. 8A. The *DCs* term describes change in  $\bar{Z}$  resulting from changes in demographic composition owing to ageing, whereas the *DCr* term describes the change in  $\bar{Z}$  resulting from the addition of new individuals owing to birth. The *VS* term is the viability selection differential on  $Z$  across all individuals; it describes how selective removal of individuals through mortality alters  $\bar{Z}$ . The contribution to  $\bar{Z}$  from age-specific trait development (growth or reversion) among individuals that survive is captured in the *GR* term. The *FS* term is the reproductive selection differential, which describes how  $\bar{Z}$  differs between parents and the unselected population. The *OMD* term represents the contribution of differences between offspring and parental trait values to  $\bar{Z}$ . The *ODC* term describes the contribution from any covariance between *OMD* and number of offspring produced by each individual. Each of these terms is weighted by demographic sensitivities, which describe how survival or reproduction in an age class contributes to population growth.

All analyses in this study were performed using the statistical and programming package, R (ref. 54).

31. Frase, B. A. & Hoffmann, R. S. *Marmota flaviventris*. *Mamm. Species* **135**, 1–8 (1980).
32. Armitage, K. B., Melcher, J. C. & Ward, J. M. Oxygen consumption and body temperature in yellow-bellied marmot populations from montane-mesic and lowland-xeric environments. *J. Comp. Physiol. B* **160**, 491–502 (1990).
33. Kilgore, D. L. & Armitage, K. B. Energetics of yellow-bellied marmot populations. *Ecology* **59**, 78–88 (1978).
34. Andersen, D., Armitage, K. & Hoffmann, R. Socioecology of marmots: female reproductive strategies. *Ecology* **57**, 552–560 (1976).
35. Melcher, J., Armitage, K. & Porter, W. Energy allocation by yellow-bellied marmots. *Physiol. Zool.* **62**, 429–448 (1989).
36. Armitage, K. B. Sociality as a life-history tactic of ground-squirrels. *Oecologia* **48**, 36–49 (1981).
37. Armitage, K. B. Reproductive strategies of yellow-bellied marmots: energy conservation and differences between the sexes. *J. Mamm.* **79**, 385–393 (1998).
38. Ozgul, A., Oli, M. K., Armitage, K. B., Blumstein, D. T. & Van Vuren, D. H. Influence of local demography on asymptotic and transient dynamics of a yellow-bellied marmot metapopulation. *Am. Nat.* **173**, 517–530 (2009).
39. Armitage, K. B. Social and population dynamics of yellow-bellied marmots: results from long-term research. *Annu. Rev. Ecol. Syst.* **22**, 379–407 (1991).
40. Armitage, K. B. & Downhower, J. F. Demography of yellow-bellied marmot populations. *Ecology* **55**, 1233–1245 (1974).
41. Schwartz, O. A., Armitage, K. B. & Van Vuren, D. A 32-year demography of yellow-bellied marmots (*Marmota flaviventris*). *J. Zool. (Lond.)* **246**, 337–346 (1998).
42. Frase, B. A. & Armitage, K. B. Yellow-bellied marmots are generalist herbivores. *Ethol. Ecol. Evol.* **1**, 353–366 (1989).
43. Woods, B. C. & Armitage, K. B. Effect of food supplementation on juvenile growth and survival in *Marmota flaviventris*. *J. Mamm.* **84**, 903–914 (2003).
44. Armitage, K. B. in *Biodiversity in Marmots* (eds Le Berre, M., Ramousse, R. & Le Guelte, L.) 223–226 (International Marmot Network, 1996).
45. Bates, D. & Maechler, M. lme4: Linear mixed-effects models using Eigen and R package v. 0.999375-32 (2009).
46. Pinheiro, J. C. & Bates, D. M. *Mixed Effects Models in S and S-PLUS* (Springer, 2000).
47. White, G. C. & Burnham, K. P. Program MARK: survival estimation from populations of marked animals. *Bird Study* **46**, 120–139 (1999).
48. Laake, J. & Rexstad, E. in *Program MARK: A Gentle Introduction* (eds Cooch, E. & White, G. C.) (<http://www.phidot.org/software/mark/docs/book/>) (2007).
49. Schluter, D. Estimating the form of natural selection on a quantitative trait. *Evolution* **42**, 849–861 (1988).
50. Kingsolver, J. G. *et al.* The strength of phenotypic selection in natural populations. *Am. Nat.* **157**, 245–261 (2001).
51. Burnham, K. P. & Anderson, D. R. *Model Selection and Inference: A Practical Information-Theoretic Approach* 2nd edn (Springer, 2002).
52. Childs, D., Rees, M., Rose, K., Grubb, P. & Ellner, S. Evolution of complex flowering strategies: an age- and size-structured integral projection model. *Proc. R. Soc. Lond. B* **270**, 1829 (2003).
53. Caswell, H. *Matrix Population Models: Construction, Analysis, and Interpretation* (Sinauer, 2001).
54. R Project for Statistical Computing. R: A language and environment for statistical computing (<http://www.R-project.org>) (2008).

## SUPPLEMENTARY INFORMATION

Table S1. Statistical models and parameter estimates describing the relationship between August 1<sup>st</sup> body mass and demographic and trait transition rates. The models include the main effects of log-body mass  $x$  and period  $p$  ( $\geq 2000$ ), and their interaction effect  $xp$ ; values in parentheses are standard errors of parameter estimates. The predicted values are the survival probability  $S$ , reproduction probability  $R$  conditional on survival, litter size  $L$  conditional on reproduction, conditional mean of log-body mass next year  $G$  given current mass, and conditional mean of log-offspring body mass next year  $Q$  given current mass. Subscripts indicate the age classes that the functions apply to. Function  $f(x | p)$  is a standard smoothing function of  $x$  including the interaction effect of  $p$  with the given degrees of freedom  $df$  for each level of  $p$ . Superscript \* indicates significance (at  $\alpha=0.05$ ) of each term based on the likelihood ratio comparison with the reduced models.  $n$  indicates the corresponding sample sizes. Logit( $Y$ ) indicates binomial regression using logit link, whereas Log( $E(Y)$ ) indicates Poisson regression using log-transformed expected values.

Function	Model	Fitted GLM / GAM	$n$
Survival probability	Logit( $S_1$ )	$-8.21_{(1.65)} + 1.25_{(0.24)} x^* - 4.59_{(4.42)} p + 0.66_{(0.64)} xp$	927
	Logit( $S_{2+}$ )	$-17.80_{(2.30)} + 2.31_{(0.29)} x^* - 14.90_{(4.71)} p^* + 1.91_{(0.59)} xp^*$	1401
Reproduction probability	Logit( $R_2$ )	$3.89_{(9.44)} - 0.68_{(1.21)} x - 43.57_{(22.27)} p + 5.50_{(2.79)} xp^*$	273
	Logit( $R_{3+}$ )	$3.08_{(7.73)} - 0.39_{(0.96)} x - 22.01_{(13.26)} p + 2.73_{(1.63)} xp^*$	604
Litter size	Log( $E(L_{2+})$ )	$-5.07_{(1.94)} + 0.74_{(0.24)} x^* - 0.83_{(3.46)} p - 0.10_{(0.43)} xp$	358
Ontogenic growth	$G_1$	$7.84_{(0.01)} + 0.11_{(0.01)} p^* + f(x^*   p^*_{df: 5.08, 2.16})$	400
	$G_2$	$4.97_{(0.53)} + 0.39_{(0.07)} x^* - 1.17_{(1.19)} p + 0.14_{(0.15)} xp$	210
	$G_{3+}$	$1.66_{(0.29)} + 0.80_{(0.04)} x^* + 1.81_{(0.48)} p - 0.22_{(0.06)} xp^*$	501
Offspring mass	$Q_{2+}$	$1.99_{(0.98)} + 0.60_{(0.12)} x^* + 0.20_{(1.76)} p - 0.02_{(0.22)} xp$	339

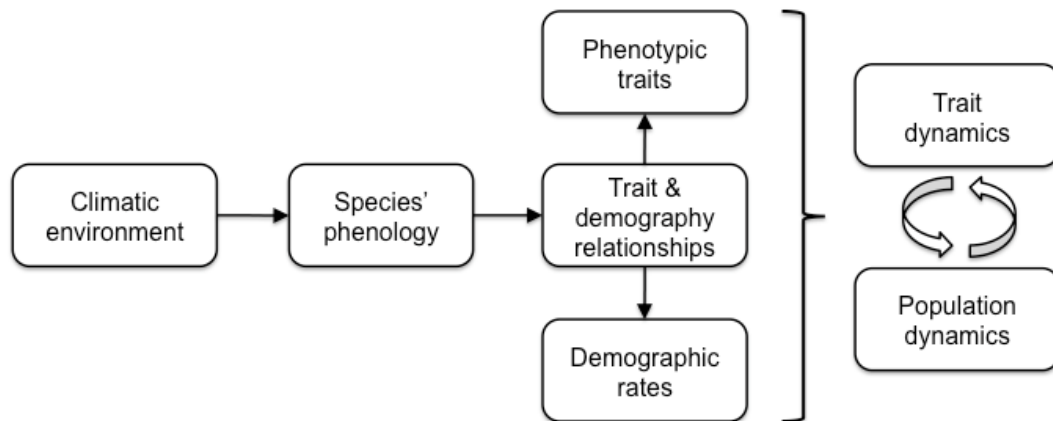


Figure S1. A change in the climatic environment can lead to a change in a species' phenology and in the relationship between traits and demographic rates. Such a change can have direct effects on the phenotypic traits (e.g., body size) and demographic rates (e.g., survival and reproduction). In this study, we demonstrate the exact mechanism through which these changes have led to a remarkable shift in the joint dynamics of population size and trait distributions in a yellow-bellied marmot population.

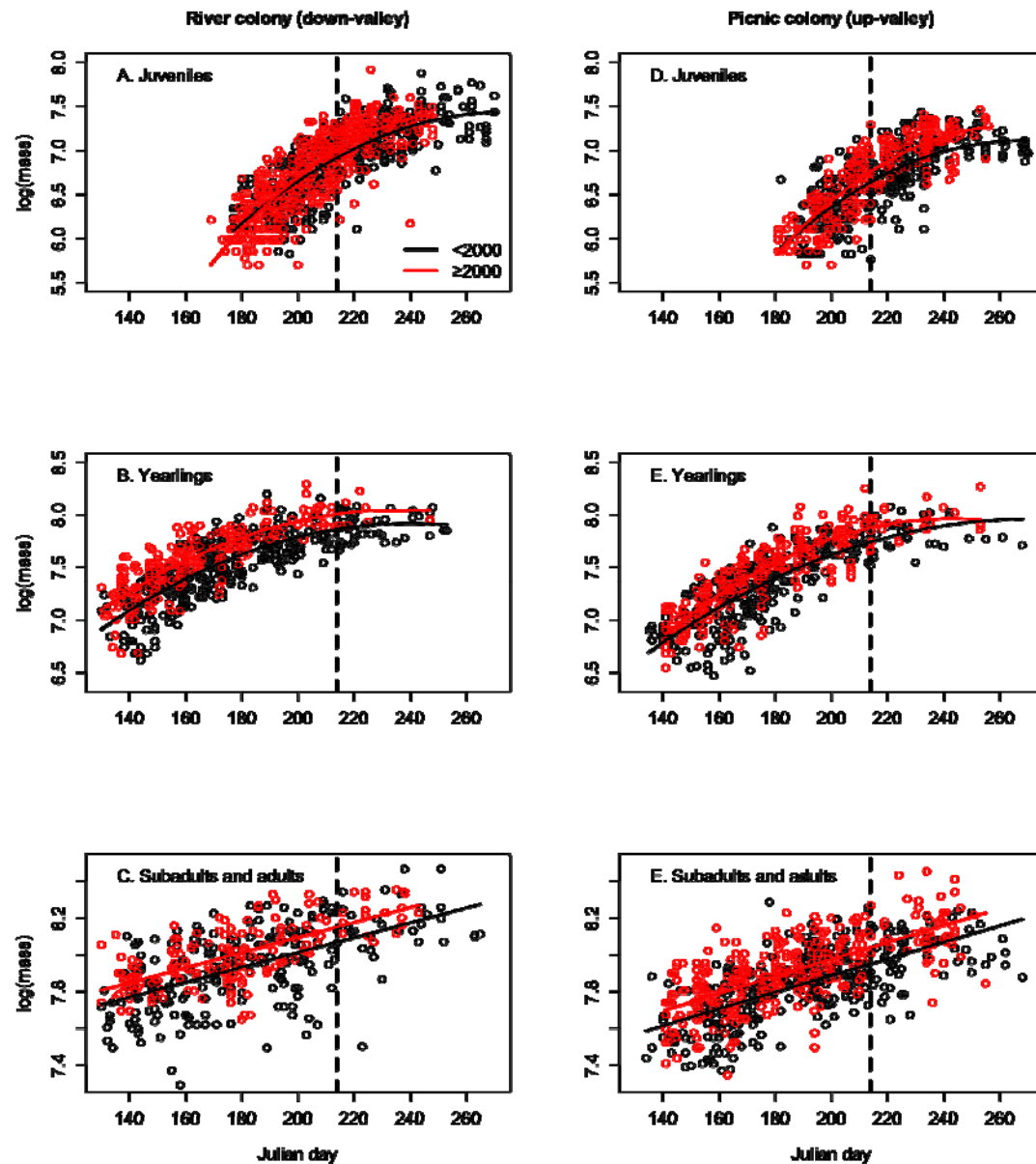


Figure S2. The relationship between day-of-year and log-body mass in two largest colony sites. The fitted mixed-effect models include quadratic relationship for juveniles and yearlings and linear relationship for older age classes. The vertical lines indicate August 1<sup>st</sup> (214<sup>th</sup> day-of-year), the date for which the body masses were estimated.

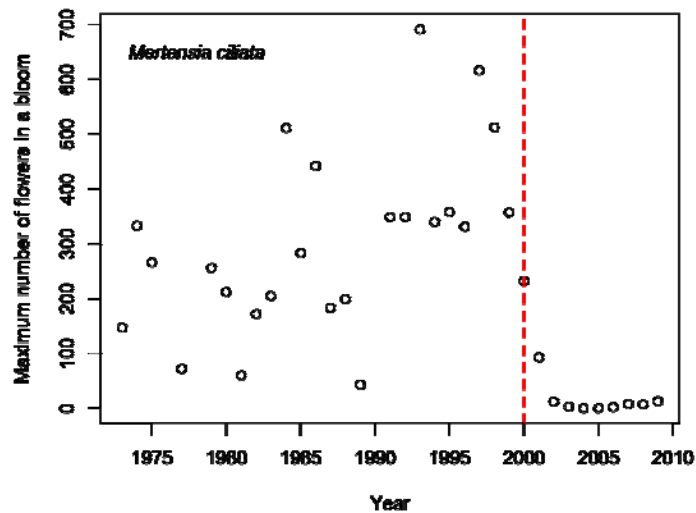


Figure S3. There has been a sharp decline in the maximum number of flowers in a bloom of the blue bell, *Mertensia ciliata*, suggesting a general environmental shift in the study area during the last decade (David Inouye, unpublished data).

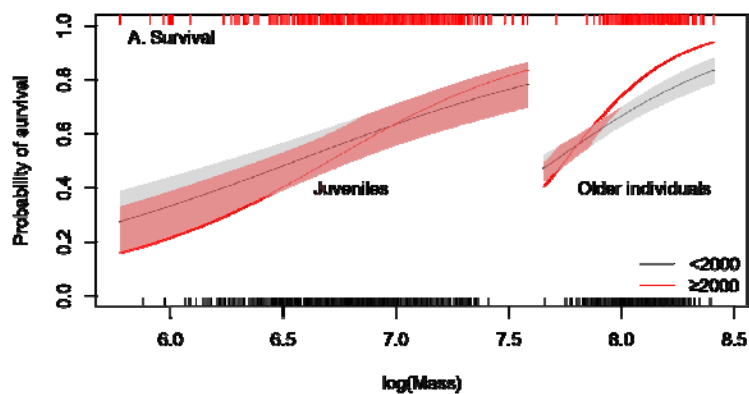


Figure S4. The relationship between body mass and survival for <2000 and ≥2000 years. Shaded areas indicate the 95% confidence intervals, and rugs above and below the graph represent the distribution of the body mass data.

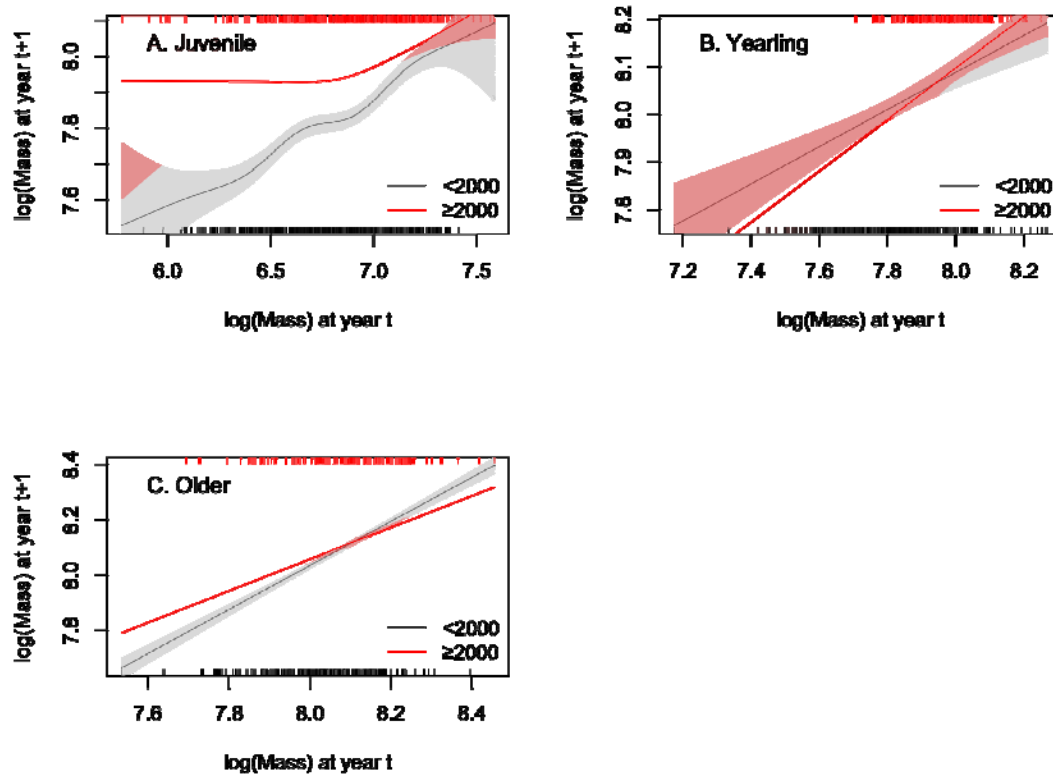


Figure S5. The relationship between body mass and age-specific growth for  $<2000$  and  $\geq 2000$  years. Shaded areas indicate the 95% confidence intervals, and rugs above and below the graph represent the distribution of the body mass data.

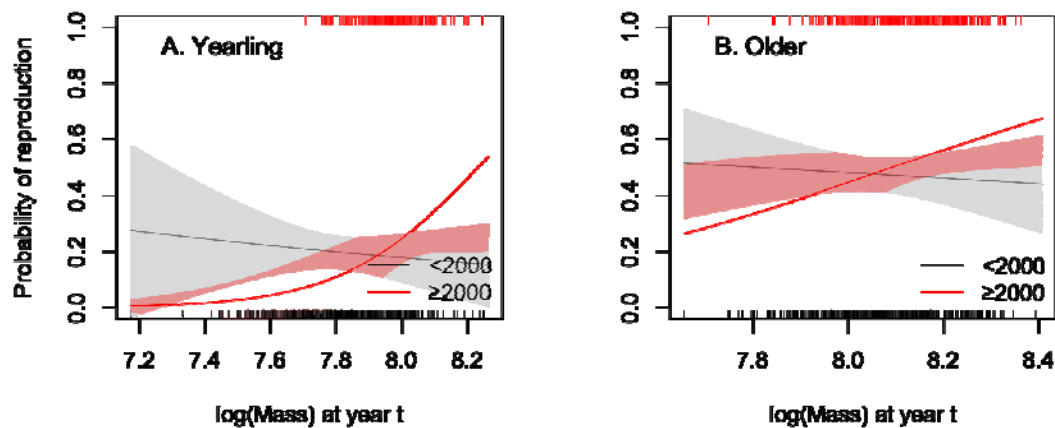


Figure S6. The relationship between body mass and age-specific probability of reproduction for  $<2000$  and  $\geq 2000$  years. Shaded areas indicate the 95% confidence intervals, and rugs above and below the graph represent the distribution of the body mass data.

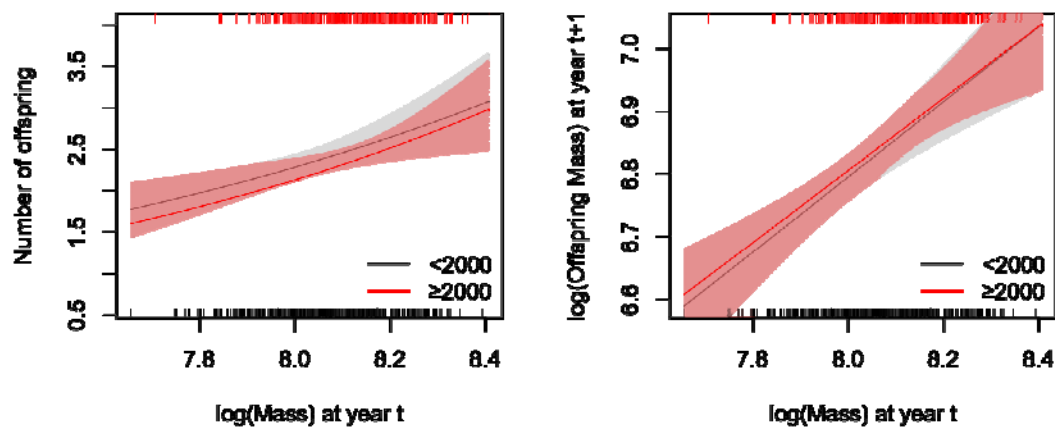


Figure S7. The relationship between body mass and (A) number of offspring produced and (B) offspring mass for  $<2000$  and  $\geq 2000$  years. Shaded areas indicate the 95% confidence intervals, and rugs above and below the graph represent the distribution of the body mass data.

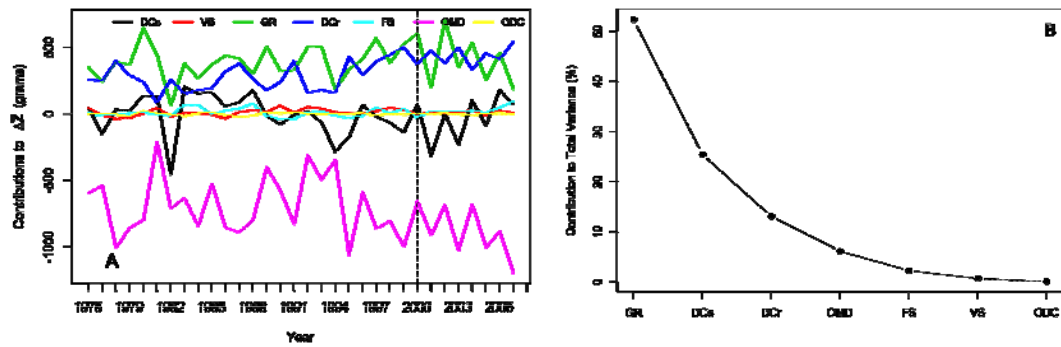
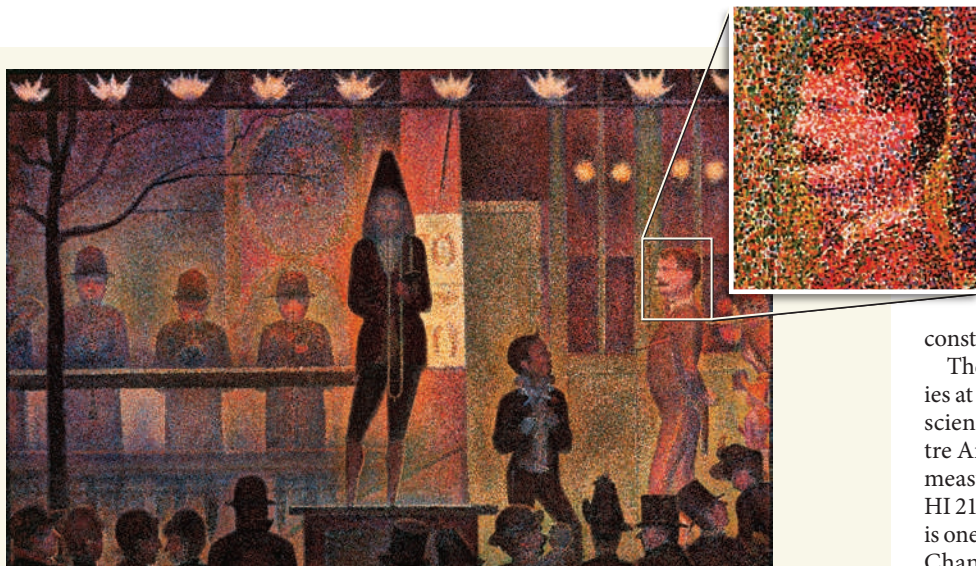


Figure S8. (A) Time-series of the contributions of different terms to  $\Delta\bar{Z}$  summed across all ages, and (B) the percentage contribution of each term to the observed total variation in  $\Delta\bar{Z}$  (see *Methods* for definition of abbreviations).



**Figure 1 | Cosmic surveys and pointillism.** Traditionally, astronomers map out the large-scale structure in the Universe by observing and cataloguing millions of galaxies — much as a painter using the technique of pointillism, here depicted in Georges Seurat's painting *La Parade de Cirque* (1888), uses many small distinct dots to generate an image. Chang and colleagues' survey<sup>3</sup> of 21-centimetre radio emission by neutral atomic hydrogen from aggregates of thousands of galaxies sidesteps the need to detect the individual sources and looks for large-scale patterns directly — somewhat like using a broad brush to produce a painting of the cosmos.

Beyond cosmology, there is astrophysical interest in determining the evolution of the neutral-gas content of galaxies. In essence, galaxy formation (to an astrophysicist) entails the conversion of gas to stars over cosmic time. The most naive assumption is that, at some point in the past, galaxies were mostly gas, which fuels star formation. But observations of this phenomenon have presented a puzzle. It is now well quantified that the cosmic star-formation rate per unit volume a few billion years ago was an order of magnitude higher than it is today. In effect, we live in a relatively

boring cosmic epoch, and things promise to become more boring with time. However, indirect measurements of the evolution of the cosmic HI mass density, through studies of HI Lyman- $\alpha$  absorption lines in the spectra of quasars and galaxies, show essentially no change in the HI mass density over this same cosmic time range and beyond<sup>9</sup>. This suggests that the gas collects in mostly molecular form ( $H_2$ ), or that the neutral atomic gas is simply seen during a phase transition as it accretes onto galaxies from the ionized intergalactic medium (or some combination thereof<sup>10</sup>).

Chang and colleagues' intensity mapping technique, coupled with surveys of optical galaxies, provides an alternative means of measuring the mean HI mass density in the distant Universe. Their result<sup>3</sup> represents an independent confirmation of the Lyman- $\alpha$  absorption measurements, supporting the conclusion that the cosmic HI mass density is roughly constant with redshift.

The detection of neutral hydrogen in galaxies at large cosmic distances has been a major science driver for the future Square Kilometre Array (SKA) radio telescope. Indeed, the measurement of the BAO by large surveys of HI 21-cm radio emission from distant galaxies is one of the key science projects for the SKA<sup>11</sup>. Chang and colleagues<sup>3</sup> demonstrate a technique that could provide the first insight into large-scale structure at high redshifts before the construction of such a mega-facility. ■ Chris L. Carilli is at the National Radio Astronomy Observatory, Pete V. Domenici Array Science Center, PO Box O, Socorro, New Mexico 87801, USA.

e-mail: ccarilli@nrao.edu

1. Peebles, P. J. E. *The Large-scale Structure of the Universe* (Princeton Univ. Press, 1980).
2. York, D. G. *et al. Astron. J.* **120**, 1579–1587 (2000).
3. Chang, T.-C., Pen, U.-L., Bandura, K. & Peterson, J. B. *Nature* **466**, 463–465 (2010).
4. Riess, A. G. *et al. Astrophys. J.* **659**, 98–121 (2007).
5. Spergel, D. N. *et al. Astrophys. J. Suppl. Ser.* **170**, 377–408 (2007).
6. Eisenstein, D. *et al. Astrophys. J.* **633**, 560–574 (2005).
7. Wetterich, C. *Phys. Lett. B* **594**, 17–22 (2004).
8. Coil, A. L. *et al. Astrophys. J.* **609**, 525–538 (2004).
9. Wolfe, A., Gawiser, E. & Prochaska, J. X. *Annu. Rev. Astron. Astrophys.* **43**, 861–918 (2005).
10. Dekel, A. *et al. Nature* **457**, 451–454 (2009).
11. Carilli, C. L. & Rawlings, S. (eds) *Science with the Square Kilometre Array* (Elsevier, 2004).

## CLIMATE CHANGE

# Fatter marmots on the rise

Marcel E. Visser

**Demonstrations of coupled phenotypic and demographic responses to climate change are rare. But they are much needed in formulating predictions of the effects of climate change on natural populations.**

Climate change is affecting natural systems, as is clear from the ample data on shifts in the seasonal timing — the phenology — of reproduction and migration, and in body size and species' distribution ranges<sup>1</sup>. Evidence that climate change is affecting population numbers is less abundant; variations in population size can have many causes. On page 482 of this issue, however, Ozgul and colleagues<sup>2</sup> describe just such a connection.

Ozgul *et al.* have studied the impact of climate change on the demographic processes affecting population numbers of yellow-bellied

marmots (*Marmota flaviventris*, pictured on the cover). These rodents live in a subalpine habitat in the United States and spend the winter hibernating. Climate change has led to a shift in the marmots' phenology of hibernation and reproduction: they now emerge earlier in spring and also wean their young earlier. As a consequence, their growing season has become longer, and they are heavier before they begin hibernation. Such shifts in phenology have been shown many times, but Ozgul *et al.* take matters further by assessing the effect that the increase in mass has had on

various demographic rates, such as winter survival and probability of reproduction. These demographic effects are then used to explain the sharp, threefold increase in marmot numbers from the year 2000 onwards.

The authors show that the marmots' demographic rates are affected in two ways by climate change. The first is a straightforward effect of the increased mass preceding hibernation. This mass directly affects winter survival, so more animals are surviving. But the second is more subtle: climate change also affects the relationship between mass and demographic processes. For instance, adult winter survival has been more strongly dependent on mass in more recent, warmer years, but, on top of that, animals have also survived better over the entire range of hibernation masses during this period than in the past. Both factors have influenced the overall increased survival. The authors use the combined effects to explain the population increase. It is fascinating that these links between phenotype and demographic processes are altering owing to climate change.

The pre-hibernation increase in mass over the study period (1976–2008) was largely due to phenotypic plasticity, as has often been found<sup>3</sup>, rather than to genetic change. This means that the marmots are not changing genetically, but that they have higher masses owing to altered environmental conditions. It remains unclear why they are now heavier. In a mechanistic approach, there is always another underlying causal level to be explored. For instance, Ruf and Arnold<sup>4</sup> showed that hibernating alpine marmots (*Marmota marmota*) that had pre-hibernation dietary access to specific plant compounds (polyunsaturated fatty acids) were able to drop their temperature at hibernation to a lower level, and hence needed less fat at the start of hibernation.

It is thus possible that, in the yellow-bellied marmot, changes in flower phenology or seed production also play a part. Interestingly, Ozgul and colleagues observed a marked decline in the number of flowers of tall bluebells (*Mertensia ciliata*), a plant included in the marmots' diet<sup>5</sup>, in the study after the year 2000. This may mean that the marmots have lacked some specific plant compounds, and so have needed to be fatter to survive hibernation. This would indicate a strategic change in hibernation mass, whereas Ozgul *et al.* assume that change is attributable simply to the prolonged growing season, and the extension of the time available for marmots to become heavier. Further insight into the complex ecological and physiological mechanisms involving energy expenditure during hibernation, winter temperature and diet during pre-hibernation fattening is needed to fully understand the observed abrupt increase in the

marmot population after 2000.

The major challenge in climate-change ecology is to predict the impact of future climate change on populations<sup>6</sup>. The study on marmots<sup>7</sup> emphasizes again that this challenge needs to be tackled with mechanistic population models that incorporate ecological and evolutionary processes<sup>7,8</sup>. In the case of the marmots, the altered ecological processes change the way in which the demographic rates are affected by hibernation mass. The evolutionary processes select for phenotypic plasticity — that is, how the environment influences hibernation mass. The task ahead is to model these processes simultaneously<sup>7,8</sup>, as well as to integrate physiology and molecular genetics into these mechanistic population models. It is only by this route that biologists will be able to forecast the implications of various climate scenarios for population viability and, ultimately, for biodiversity. ■

Marcel E. Visser is at the Netherlands Institute of Ecology (NIOO-KNAW), PO Box 40, 6666 ZG Heteren, the Netherlands.

e-mail: m.visser@nioo.knaw.nl

1. Parmesan, C. *Annu. Rev. Ecol. Evol. Syst.* **37**, 637–669 (2006).
2. Ozgul, A. *et al.* *Nature* **466**, 482–485 (2010).
3. Gienapp, P., Teplitsky, C., Alho, J. S., Mills, J. A. & Merilä, J. *Mol. Ecol.* **17**, 167–178 (2008).
4. Ruf, T. & Arnold, W. *Am. J. Physiol. Regul. Integr. Comp. Physiol.* **294**, R1044–R1052 (2008).
5. Frase, B. A. & Armitage, K. B. *Ethol. Ecol. Evol.* **1**, 353–366 (1989).
6. Jenouvrier, S. *et al.* *Proc. Natl Acad. Sci. USA* **106**, 1844–1847 (2009).
7. Visser, M. E. *Proc. R. Soc. B* **275**, 649–659 (2008).
8. Chevin, L.-M., Lande, R. & Mace, G. M. *PLoS Biol.* **8**, e1000357 (2010).

## CATALYSIS

# Fluorination made easier

Tobias Ritter

**By putting the pieces of a chemical puzzle into the right order, a thorny problem in catalysis has been solved. This opens the door to syntheses of molecules that contain the useful trifluoromethyl group.**

When chemists try to make molecules, they cannot always get what they want. For example, they have tried for some time now to find good ways of introducing trifluoromethyl groups (CF<sub>3</sub>) into complex organic molecules, but without much success. There are compelling reasons to develop such a reaction, because the introduction of trifluoromethyl groups can dramatically change the properties of molecules, often for the better. Among other things, trifluoromethyl groups can increase the brain penetration of drugs that act on the central nervous system, and they can make materials more durable. Reporting in *Science*, Cho *et al.*<sup>1</sup> now describe a general catalytic reaction that allows molecules containing trifluoromethyl

groups to be made much more easily than before.

Although trifluoromethyl groups have been known for a long time, the preparation of molecules that contain them has been challenging. This is because many of the synthetic methods for making these molecules required harsh reaction conditions such as high temperatures, which can be applied only to fairly simple molecules (which are often the most robust). For the synthesis of more complex trifluoromethylated molecules, one needed to start from a simple, readily available molecule that contains a trifluoromethyl group and then build up the desired molecule from it, a process that can be lengthy and time-consuming.

Nevertheless, because trifluoromethyl groups have been so successful in improving various molecules' properties, perhaps most notably the biological properties of drugs, chemists were willing to go the extra mile. The antidepressant fluoxetine (Prozac), for example, contains a trifluoromethyl group; dutasteride (Avodart), a drug that changes the processing of testosterone in the body, even has two. But the synthetic rules were simple: don't bother trying to attach a trifluoromethyl group to a complex molecule, because success is extremely unlikely.

With the advent of Cho and colleagues' reaction<sup>1</sup>, the rules could be about to change. The authors have tackled this synthetic challenge by using palladium-catalysed cross-coupling chemistry, a field that has been around for almost 50 years. Cross-coupling catalysis, in which two molecular fragments are joined together with the assistance of a metal catalyst, has transformed, hands down, the way in which chemists build molecules<sup>2</sup>. One reason for its success is that it is simple to identify how cross coupling can be used when devising a synthetic route for a target molecule. Developments over the past few decades have increased the efficiency and reliability of cross-coupling catalysis to such an extent that it is now hard to find a synthesis of a drug-like molecule that does not use this chemistry.

So why has it taken so long to develop cross-coupling reactions for trifluoromethyl groups? After all, the group is simply a methyl group (CH<sub>3</sub>) in which all three hydrogen atoms have been replaced with fluorines, and highly effective cross-coupling methods for attaching methyl groups to molecules have been available for some time. The answer is that the electronic properties of fluorine atoms are very different from those of hydrogen atoms, which makes trifluoromethyl groups much less reactive than methyl groups for cross-coupling reactions. What's more, trifluoromethyl groups are more prone to undergoing undesired side reactions in cross-coupling processes.

Enter Cho *et al.*<sup>1</sup>, who have used simple chemicals known as aryl chlorides (Fig. 1) as starting materials for their reactions. These compounds are readily available, in part because they are widely used in other cross-coupling processes. In the authors' trifluoromethylation reaction, aryl chlorides react with a palladium catalyst, forming intermediate compounds in which a palladium atom has inserted itself into the carbon–chlorine bond of the aryl chloride so that the palladium is bound to both the carbon and the chlorine atoms (Fig. 1a). In the next step of the catalytic cycle, exchange of the chlorine for a trifluoromethyl group (provided by another starting material) generates another palladium intermediate (Fig. 1b), from which the desired product — in which the chlorine atom of the aryl chloride has been replaced with a trifluoromethyl group — forms (Fig. 1c). The overall process is therefore the replacement